15TH IEA HEAT PUMP CONFERENCE
MAY 26–29, 2026 | HOFBURG
VIENNA 2026
DECARBONISATION THROUGH INNOVATION

Strategies for reducing and detecting frost formation on air source heat pumps

Sabine Apelt[a*], Chenglin Li[a], Anne Feuer[b], Ravil Idrisov[b], Kilian Tschöke[c], Patricia Stelle[c], Daniel Roy[d], Ute Bergmann[a]

[a]Institute of Materials Science, Technische Universität Dresden, 01062 Dresden, Germany
[b]Fusion Bionic, Löbtauer Straße 69, 01159 Dresden, Germany
[c]Fraunhofer Institute for Ceramic Technologies and Systems IKTS, Maria-Reiche-Str., 01109 Dresden, Germany
[d]WiE GmbH, Am Mühlgraben 3, 01731 Kreischa, Germany

Abstract

Air source heat pumps (ASHPs), the most widely used heat pump type in residential buildings across Europe, suffer efficiency losses in cold, humid conditions due to frost accumulation on their evaporator surfaces. Frost forms in stages: humid air first condenses into water droplets, which then freeze and accumulate into an insulating frost layer that reduces heat transfer, increases pressure drop, and necessitates defrosting. These effects lower the system's coefficient of performance (COP).
This work explores both passive and active strategies to mitigate frost formation and improve frost management. Passive approaches include surface functionalization through laser structuring and coatings, aiming to reduce condensation, water accumulation and control frost distribution under mild conditions. In harsher conditions, where frost formation is unavoidable, reducing ice adhesion strength becomes more critical—potentially allowing mechanical methods such as piezoelectrically induced elastic waves to dislodge ice with minimal thermal input.
An experimental setup has been developed to observe frost formation in situ on various surfaces under defined conditions. The tests presented in this article include bio-inspired microstructure such as superhydrophobic surfaces and topographies found on Arctic scallop shells, assessed for its potential to influence frost thickness and ice adhesion. Surface properties such as laser structure, contact angle and contact angle hysteresis are being correlated with observed icing behavior. In parallel, we investigate piezoelectric detection strategies for water and ice to enable predictable, demand-specific defrosting. Conventional time- or temperature-based control often leads to premature or delayed defrost cycles. By using sensors, defrosting can be triggered more efficiently, reducing unnecessary energy consumption. The combined approach of detecting and reducing frost formation offers promising insights into smarter anti-ice strategies for next-generation ASHP systems.

Keywords: ASHP, evaporator, defrosting;

1. Introduction

After industry, transportation, and the energy sector, heating in buildings is the fourth largest source of greenhouse gas emissions in Germany. In order to achieve the climate targets, the share of heat generators based on renewable energies must be significantly increased from the current level of around 22 %. Heat pumps, especially when powered by renewable electricity, cause significantly fewer greenhouse gas emissions than the oil and gas heating systems that are still most commonly used today [1]. Heat pumps are usually categorized according to their heat source, including groundwater, ground-source and air-sourced heat pumps. Due to their lower installation costs compared to water-sourced heat pumps, air-sourced heat pumps (ASHPs)

* Corresponding author. Tel.: +49 351 463 34895
E-mail address: sabine.apelt@tu-dresden.de

are the most widely used, especially when retrofitting existing buildings. However, one disadvantage of this technology is that its efficiency is highly dependent on climatic conditions. Air temperatures below 7 °C combined with high humidity can lead to frost forming on the evaporator, reducing heat transfer and causing a significant increase in pressure loss [2,3]. In this work, ASHP refers exclusively to air-to-water heat pumps (outdoor-air source with a water-based heating system for space heating and, where applicable, domestic hot water); air-to-air systems are out of scope.

This paper reports on ongoing research in a project aimed at increasing energy efficiency in ASHPs by combining active and passive anti-icing strategies. At the time of writing this manuscript, tests on the combination of active and passive de-icing strategies on a real heat pump had not yet been completed. A final evaluation of the results will be provided in the project final report.

1.1. Active anti-ice strategies for evaporators

So-called active strategies against unwanted ice and frost adhesion include heating, mechanical removal, or the use of de-icing chemicals. Chemical de-icing agents are used on car windows and aircrafts as well as in large-scale industrial cooling and air conditioning systems, but are viewed as problematic in ASHPs due to cost and environmental toxicity concerns. Electro-thermal heating is the most common strategy to remove ice and frost from ASHP evaporators by heating the surface above the melting temperature. However, this either consumes electrical energy for heat generation, which reduces the coefficient of performance (COP) of the heat pump, or uses the heat from the building via cycle reversal for defrosting, whereby no heating capacity is available during the defrosting process [4]. The primary focus of research in this area is currently on determining the optimal start time and duration of defrost cycles as function of the outdoor conditions [5]. The third option is to remove the ice mechanically without additional heat or chemical input.

Different methods for de-icing a surface using piezoelectric transducers are suitable for use on evaporators. The first method uses the generation of eigenmodes of a structure for de-icing [6]. Eigenmodes are characteristic vibration patterns that occur at specific frequencies, reflecting distinct shapes and motions of the plate associated with its resonance behavior. The piezoelectric transducer must be selected in terms of shape and size so that its thickness resonance frequency matches the eigenfrequencies of the structure. A second approach relies on resonance vibrations of the piezoelectric transducer, but not on its thickness vibration, rather on its radial vibration. This radial resonance must be selected so that the induced vibration overcomes the tensile strength of an ice layer [7]. A third method involves the targeted generation of shear waves, whose displacement ultimately overcomes the shear strength of an ice layer and thus removes the ice [8-10]. Ramanathan et al. [8] specifies a shear force of 0.15 MPa to 1.6 MPa that must be overcome to detach ice from the surface of a steel plate.

The effectiveness of active defrosting strategies in air-source heat pumps critically depends on reliably detecting the presence of water and ice on the fin surfaces [11]. In current systems, such detection is achieved predominantly in an indirect manner [5]. Piezoelectric transducers are promising components for application in ASHPs because they can operate both as sensors for the detection of water and ice (piezoelectric effect) and as actuators for active de-icing (inverse piezoelectric effect). In the present work, the focus is initially placed on the detection of liquid water on the fins, while the detection of ice and its mechanical removal are defined as subsequent objectives of the ongoing project.

1.2. Passive anti-ice strategies for evaporators

Passive anti-icing strategies aim to minimize ice and frost formation through appropriate geometrical and surface design of the evaporator fins, without any additional expenditure of electrical energy or chemicals. Choosing a fin geometry that causes turbulent flow and optimized fin spacing can reduce frost formation. Structuring and coating of surfaces is used to delay the onset of ice formation and/or minimize the adhesion of ice layers that have already formed, while ensuring that the surface modification has the longest possible service life. Figure 1 shows the stages of water condensation from the surrounding humidity, growth and coalescence of the water droplets, freezing and frost layer growth. The amount of accumulated water and ice is not only determined by the humidity of the surrounding air but also by the adhesion of water and ice on to the surfaces. To minimize the accumulation of water and thick layers of frost on the evaporators, the surface should be designed to be both water- and ice-repellent.

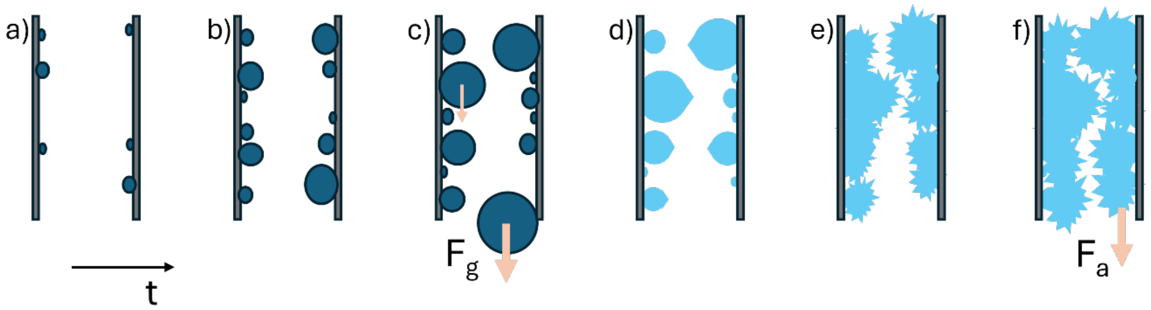

Figure 1. On freshly defrosted fins in ASHP or when the surface temperature of the evaporator is in the borderline region between condensation and frosting, a) tiny water droplets initially form from the surrounding moist air due to condensation. These droplets b) grow and coalesce with neighboring droplets. c) When the droplets reach a certain size, their weight causes some of them to run down the fins due to gravitational forces. d) If heterogeneous nucleation occurs, the first droplets freeze and the ice front spreads to neighboring droplets until all droplets are frozen. e) Now the moisture settles on the droplets as frost needles and f) the frost layer continues to grow, causing the flow paths through the evaporator to become increasingly narrow. Points of intervention are c) for water removal by gravitational force F_g and f) for ice removal by piezoelectric induced shear waves that overcome the ice adhesion F_a.

Many of the modifications already used for this purpose are inspired by naturally occurring surfaces [12], with the superhydrophobicity of lotus leaves being the most frequently studied to date, since superhydrophobic surfaces are known to improve the performance compared to e.g. hydrophilic surfaces [13]. On superhydrophobic surfaces, the hierarchical structures enable contact angles >150 °, thus minimizing the contact area between the water droplets and the evaporator surfaces [14]. The possibilities for changing the wettability of fin surfaces range from sodium hydroxide solution etching followed by fluorination [15] to coating fins with nano-protrusions with fluorinated resin [16]. Superhydrophobic surfaces can only be achieved through a combination of hierarchical structuring and chemical modification to reduce surface energy. Direct laser interference patterning (DLIP) is a promising method for applying periodic biomimetic structures with narrowly defined dimensions at industrially relevant speeds over large areas. The DLIP process is based on the principle of interference between overlapping laser beams, which results in a periodically modulated distribution of laser intensity [17]. Therefore, DLIP is a promising and reliable method for the rapid and large-scale laser production of clearly defined periodic micro- and nanostructures on surfaces. Typically, the hierarchically structured surfaces are then coated with a thin layer of materials that have low surface energy. Due to severe ecological and physiological concerns, intensive research is currently being conducted into alternatives to the perfluorinated and polyfluorinated alkyl compounds (PFAS) commonly used for the chemical modification of structured surfaces, which are necessary to achieve superhydrophobic properties [18].

To date, it has not been possible to completely prevent evaporator surfaces from icing up in all possible temperature and humidity conditions using passive anti-icing strategies alone. Therefore, active and passive strategies should always be combined whenever possible [19]. The aim of this study is to investigate various PFAS-free surface modifications by DLIP and polydimethylsiloxane (PDMS) coating to determine whether, due to their hydrophobicity, they allow condensing water to run off more easily, while at the same time leading to thinner frost layers under moderate conditions and exhibiting low ice adhesion to already formed ice, making it easier in the future to remove the ice using piezoelectric transducers for mechanical de-icing.

2. Materials and Methods

2.1. Sample preparation

As a substrate material, cold-rolled aluminum sheets with a purity of 99 % (Güntner GmbH, Germany) and a thickness of 0.15 mm were used. The sheets were cut into samples of different sizes depending on the characterization method. For structuring the aluminum sheets with dot-like and pillar-like structure geometries, the DLIP optics CORErapid IR30.4 from Fusion Bionic and the laser system TruMicro 6020 from TRUMPF were used. The laser system operates at a wavelength of 1030 nm and a pulse duration of 3 ps and provides a maximum average power of 200 W. The spatial period of the interference maxima generated with the CORErapid IR 30.4 was set to 15 µm. The dot-like surface structure was obtained by setting the pulse spacing to an integer multiple of the spatial period and the resulting surface structure consists of regularly arranged individual dimples with a spacing of approx. 15 µm and a depth of 5 µm - 10 µm. The generation of the pillar-like surface structure was conducted in two sequential steps. First, a line pattern was generated by employing a pulse spacing smaller than the spatial period. Subsequently, the scanning direction was rotated by 90°, and the remaining peaks were selectively ablated. A depth of approximately 10 µm was also generated for the pillar-like structure. The coating solution was prepared with 89 wt-% isopropyl alcohol (VWR Chemicals), 10 wt-% PDMS and 1wt-% sulfuric acid (VWR Chemicals). PDMS was purchased from Gelest Mitsubishi Chemical Group with a molecular weight of 9430 g/mol. The solution was stirred for 30 s and left to stand for 30 min before being used for the dip-coating process. The aluminum samples were immersed in the coating solution for 10 s before being withdrawn with a constant speed of 0.5 cm/s. The samples were placed in an oven at 75 °C for 20 min for curing. The thickness of the coating produced is significantly smaller than the structural depth of the laser processing. After coating, the protrusions in the µm range remain, but the PDMS fills most of the nm-scale irregularities that were also created by the laser processing [12].

2.2. Static and dynamic contact angle

The static and dynamic contact angles were measured with the OCA15 (Dataphysics Instruments GmbH). At least 10 droplets of deionized water with a size of 2 µl were placed subsequently on different positions on the sample surface and the static contact angle was measured for each droplet using the dataphysics software SCA20 after a 10 s-waiting time. The dynamic contact angle was measured at least 10 times by injecting and withdrawn 2 µl of deionized water from a pre-existing 2 µl droplet at a rate of 0.2 µl/s. A 2 s-interval was maintained between the cycle that was repeated at least 10 times. The contact angle hysteresis was calculated by averaging the difference between the maximum and minimum contact angle in each cycle.

2.3. Ice adhesion

To measure the shear stress that must be overcome to remove ice from a surface, a pusher test inside a climate chamber (ESPEC) as described by Apelt and Bergmann [20] was used. A volume of 320 µl of deionized water was filled into an aluminum mold placed on top of the samples covering a surface area of 78.54 mm^2. The temperature inside the climate chamber was reduced to -10 °C at a rate of 1 K/min. After a holding time of at least 90 min to ensure freezing of the water and a homogenous temperature distribution throughout the sample, the aluminum mold was pushed horizontally at a rate of 2 mm/s. The required force and displacement were recorded with two different sensors and the ice adhesion was calculated from the force maximum measured during a sudden displacement of the aluminum mold for at least 6 independent samples per surface modification.

2.4. Frost layer thickness

A combined cooling and camera system was set up in a climate chamber (FDM) to analyze frost growth on the different samples. To simulate the conditions in an ASHP under icing conditions, the climate chamber was set to an air temperature of 7 °C and a relative humidity of 50-60 %. The flat samples were vertically attached to a controllable cooling plate (Linkam Scientific Instruments Ltd.) using self-adhesive thermos pads. The cooling plate were chosen to be slightly smaller than those of the sample in order to reduce the influence of non-uniform environmental conditions during frosting that can arise from incomplete contact between the sample edges and the cooling plate. The Linkam cooling plate was first set to a temperature slightly above the dew point and hold there for 30 min to ensure homogenous temperature distribution in the measurement setup. With a cooling rate of 5 K/min the temperature of the cooling plate was then set to -12 °C (cooling rate 5 K/min) and held there for 90 min before being heated again to 10 °C. During this time, the samples were simultaneously observed with a front camera, a macro camera, and an infrared camera. The macro camera was focused on the side of the sample. The videos from the macro camera were used afterwards to quantify the temporal progression of frost growth per measurement cycle using automated image analysis as shown in Figure 2. The frost thickness maximum was determined from the images at the end of the 90 min holding time at -12 °C. All frosting experiments were performed with only natural convection and no externally imposed air flow. To minimise radiative heat exchange from external light sources, the glass door of the climate chamber was shielded with a black cover. Illumination inside the chamber was provided only by a 5 W cold-light ring lamp operated at its lowest intensity level. For frost-thickness measurements, we first calibrated the pixel-to-length scale using the sample before icing by recording the pixel length corresponding to a known sample thickness of 0.15 mm. At the time of maximum frosting, 15-20 measurement points were selected at approximately equal intervals across the field of view and extracted the pixel lengths of the local frost thickness, then these pixel values were converted to physical thickness using the calibration. Since the measurement includes frost on both sides, the single-side thickness was computed as half of the two-sided value after subtracting the substrate thickness. At least four subsequent cycles were performed for each surface modification and the thickness values were averaged.

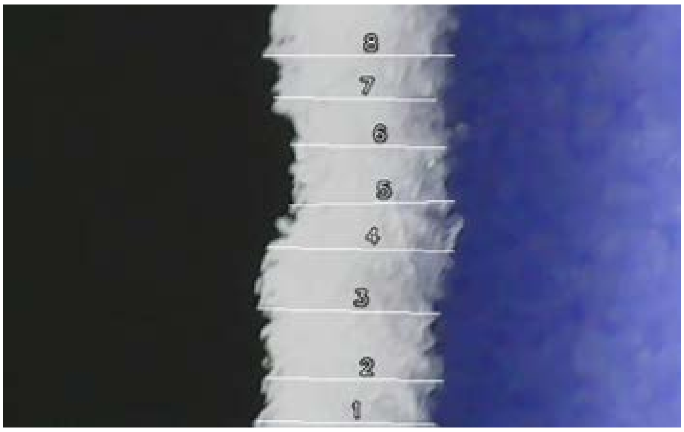

Figure 2. Determination of the average frost thickness on the sample surfaces after 90min frosting time as average value at multiple measurement points in the perpendicular macro image of the samples fixed with a blue thermopad on top of the cooling stage.

2.5. Piezoelectric water detection

Piezoelectric transducers can be used not only for mechanical de-icing, but also for detecting water and ice on the fins of heat exchangers, for example by means of electromechanical impedance analysis. As part of the electromechanical impedance analysis, the transducers are examined under small-signal alternating current load and the complex electrical resistance is measured. The results reveal a correlation between the electrical properties of the piezoceramics and the mechanical properties of the object (transducer + fin + water/ice). In order to obtain a measure of the subsequent water layer thickness, two signals from an impedance measurement on a transducer must be compared with each other. These are the so-called baseline, the measurement signal without water droplets, and the measurement signal of the condition with water droplets. It is known from the literature that the susceptance in particular is a suitable measurement variable for detecting deviations around and on a piezoelectric transducer in the context of impedance analysis [21]. For this reason, the correlation coefficient of the susceptance curves of the baseline and measurement signal with 75µl water droplets positioned on different positions in the surrounding of the transducer is used as an index (here called damage index) to determine a deposit.

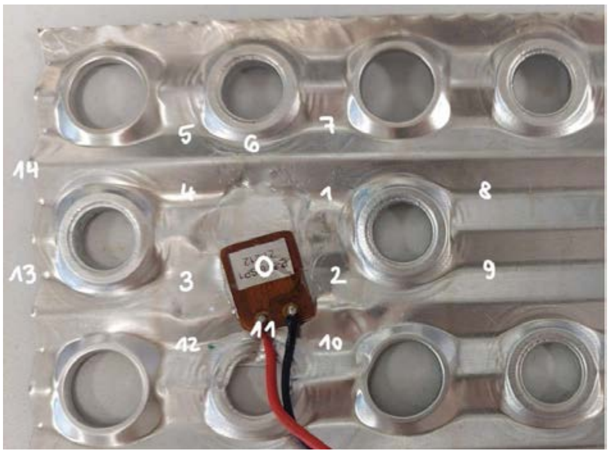

Figure 3. Applied piezoelectric transducer on a heat exchanger fin. The positions for the impedance measurements are marked.

Figure 3 shows an example of a piezoelectric transducer applied to a heat exchanger fin in the laboratory. This is a DuraAct transducer of type SP1 from PI Ceramic GmbH, applied to the fin using two-component epoxy adhesive. Around the transducer, water droplets of varying sizes were applied to 14 positions in succession. In order to compensate for random influences during the measurements, a series of 5 measurements was carried out for each of the 14 positions and the damage indices were averaged.

3. Results and Discussion

To investigate the influence of DLIP and PDMS coating of fins on icing behavior, thin sheets of pure aluminum were structured using DLIP with either dots or pillars. Some of the structured samples were then coated with PDMS, and the icing behavior was compared both with the reference aluminum samples and with aluminum samples that were only coated with PDMS. To test the mechanical stability of surface modifications, some surface properties were determined again after three subsequent mechanical de-icing tests (referred to as "wear" in the figures).

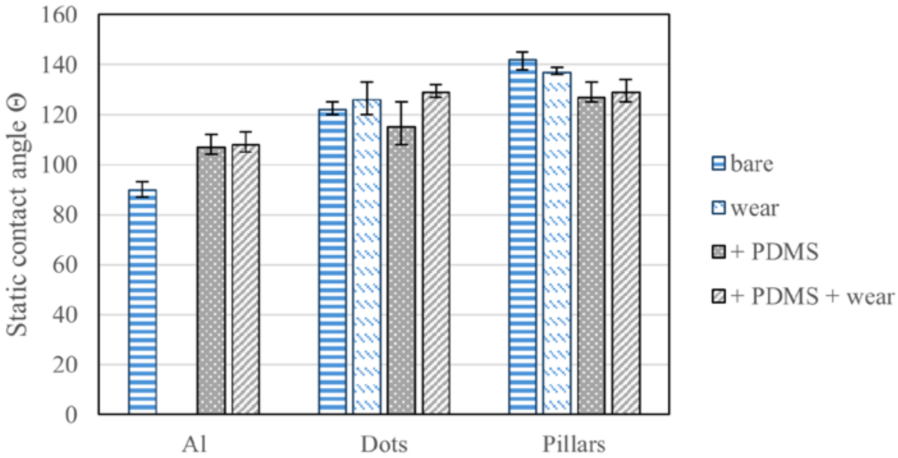

Figure 4. Median values for the static contact angle on bare Al, Al structured with dots and Al structured with pillars; with and without an additional PDMS coating, once measured directly after the manufacturing and once after three rounds of ice adhesion testing (wear)

The results of the static contact angle measurements are shown in Figure 4. DLIP structuring increases the hydrophobicity significantly compared to bare aluminum due to the micro- and nano-topography as result of the laser ablation. The dot and pillar structures exhibit the same periodicity of micro-structuring and similar nano-structuring, but in the dot structure, material is removed in the specified periodicity, whereas the pillar structure is the negative of the dot structure and material remains at specific points due to double structuring with lines. Overall, more material is removed in the pillar structure and, despite the same periodicity, higher static contact angles are achieved. After repeated de-icing, it can be seen that the dot structure is more resistant, with the contact angles remaining comparably high, while the pillar structure shows a slight decrease in hydrophobicity.

For bare aluminum, a subsequent PDMS coating leads to higher contact angles due to the reduced surface energy. In contrast, the PDMS coating reduces the contact angles on DLIP surfaces. The thin PDMS layer fills some of the grooves in the structured surface, but does not completely cover the hierarchical structure as was also shown in [12]. After multiple mechanical de-icing cycles, the PDMS-coated dot structures again exhibit contact angles that are just as high as those of uncoated dot structures. In the case of pillar structures, the contact angles of the PDMS-coated pillars remain the same even after multiple de-icing cycles.

In addition to the static contact angle, contact angle hysteresis (CAH) is also an important parameter for characterizing the wettability of surfaces. CAH describes how the contact angles differ between the wetting of previously unwet areas and the de-wetting of previously wet areas when the contact line between the water drop, the surface, and the surrounding air moves. On surfaces with smaller CAH, less force is required to move water droplets across the surface. The results of the CAH measurement are shown in Figure 5. Pure aluminum exhibits comparatively high CAH values, which means that water cannot be removed from the surface as easily. Coating with PDMS and, in particular, repeated mechanical de-icing of this PDMS coating further increases the CAH. It is likely that repeated de-icing has caused defects in the coating, leading to pinning of the water droplets and thus to high CAH.

Hierarchical structures generated by DLIP lead to significantly reduced CAHs. In dot structures, multiple mechanical de-icing leads to deterioration, whereas in pillar structures, multiple mechanical de-icing actually reduces CAHs even further. Coating with PDMS does not initially lead to any significant deterioration in CAH, but repeated mechanical de-icing causes defects on the surface that promote water adhesion. This behavior is independent of whether the surfaces were structured with dots or pillars prior to PDMS coating.

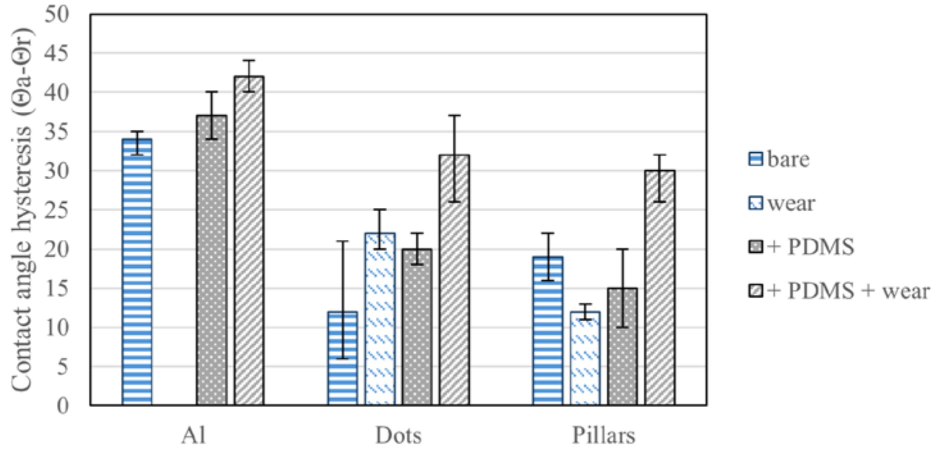

Figure 5. Median values for the static contact angle hysteresis (CAH) on bare Al, Al structured with dots and Al structured with pillars with and without an additional PDMS coating, measured directly after manufacturing and after three rounds of ice adhesion tests (wear)

Figure 6 shows the results of the frost thickness measurement on the different samples. The conditions (air temperature, relative humidity, surface temperature of the samples) were selected so that they could be kept stable in the existing FDM climate chamber for the entire measurement period and also corresponded to conditions that approximate those found in real ASHPs. At outside air temperatures between +7 °C and -5 °C, the necessary defrost cycles cause the greatest efficiency losses in ASHPs. At even lower temperatures, the energy required for defrosting increases further, but the absolute humidity of the outside air is then so low that frost formation on the evaporator is virtually eliminated. The conditions in the present experiments were also chosen so that the surface is located in the boundary area between the condensation region and the frosting region of the condensation frosting performance maps [22].

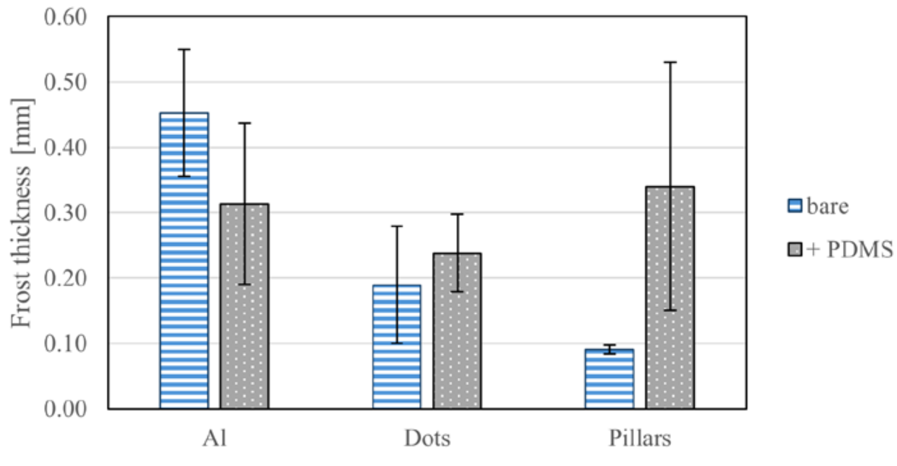

Figure 6. Frost thickness on bare Al, Al structured with dots and Al structured with pillars with and without an additional PDMS coating after 90 min in frosting conditions (7°C air temperature, 45-60% relative humidity, -12°C cooling plate temperature)

After a constant period of 90 minutes and under identical frost conditions, significantly less frost formed on the DLIP surfaces compared to the bare Al samples. The pillar structure even exhibits lower frost layer thicknesses than the dot structure. This phenomenon is usually explained by the fact that water is more easily removed from the surface during the condensation phase [13], resulting in a smaller overall frost thickness, even though wettability no longer influences the behavior of the droplets and frost formation once freezing has occurred on the surface (Figure 1). The individual surface properties, such as contact angle and CAH, show different trends in their influence on the icing behavior of ASHP evaporators (Figure 7). The correlation of the frost thickness with the static contact angle seems more pronounced compared to the correlation of the frost thickness with CAH.

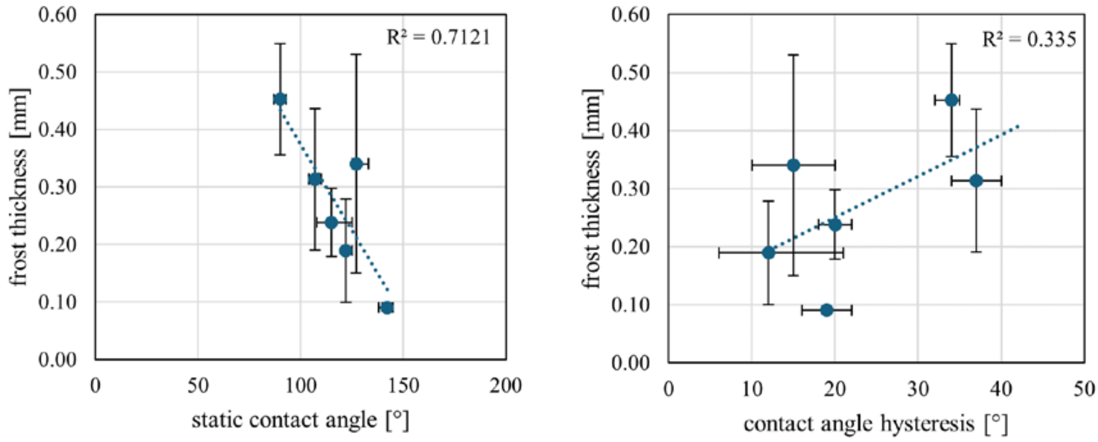

Figure 7. Possible correlations between the frost thickness and the surface properties of the different samples.

The lateral adhesion force F_l required to slide a water droplet over a surface follows equation (1) where w is the width of the contact area of the drop, γ_L is the surface tension of water and $k \sim 1$ is a geometrical factor, which depends on the shape of the drop [23]. Consequently, in addition to a minimized contact angle hysteresis CAH $(\Theta_a$-$\Theta_r)$, a high contact angle is also necessary to minimize the width of the contact area w to achieve low lateral adhesion forces. Then, the gravitational force $F_g = m \cdot g$ is enough to remove even small water droplets with low mass m from the evaporator surface (Figure 1).

$$F_l = w \cdot \gamma_L \cdot k \cdot (cos\theta_r - cos\theta_a) \quad (1)$$

Compared to the pillar structure, the dot structure has a slightly higher contact angle and comparable CAH resulting in an overall thinner frost layer thickness after 90 minutes. However, in addition to the contact angle and CAH, there must be other influencing factors that have not yet been identified here. The PDMS-coated dots and pillars structures also continue to exhibit increased contact angles and small CAH, but the resulting frost layer thickness settles at comparable values, regardless of whether the PDMS layer was applied to bare aluminum or aluminum sheets with DLIP structures as shown in Figure 6.

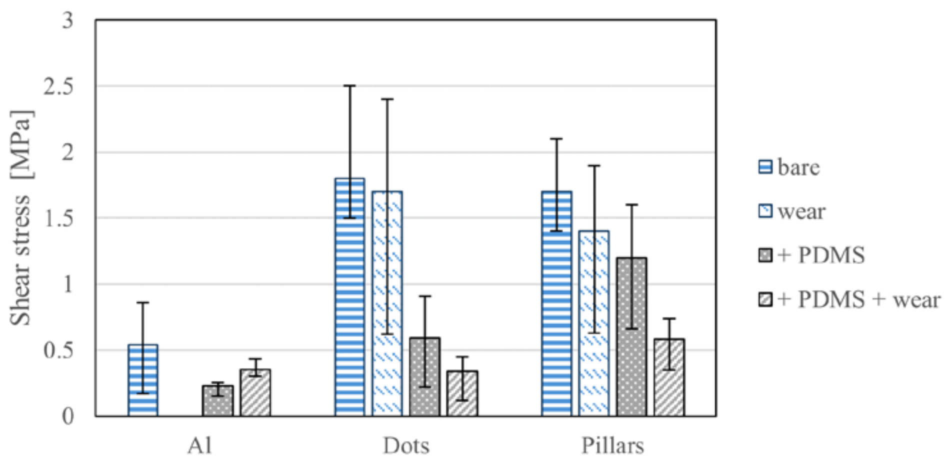

Figure 8. Median values for the ice adhesion strength on bare Al, Al structured with dots and Al structured with pillars with and without an additional PDMS coating, measured directly after the manufacturing and after three rounds of ice adhesion testing (wear)

Under frosting conditions in ASHPs, water remains in its liquid form for only a fraction of the time before it freezes and forms layers of frost. To prevent the associated pressure loss, the ice must either be thawed or removed using mechanical force, e.g., by piezoelectrically induced shear waves. The greater the ice adhesion, the greater the shear forces required and thus also the energy required to excite the piezo transducers. Laser structuring of aluminum with dot and pillar structures reduces water adhesion, but the micro- and nanostructures significantly increase the shear force required to remove ice once it has formed on the surface (Figure 8). Subsequently coating the structured surfaces with PDMS and similar silicone coatings is known to reduce ice adhesion, but the often highly elastic layers are subject to severe abrasion. Ice adhesion on PDMS-coated surfaces increases with repeated mechanical de-icing, most likely caused by partial destruction of the coating. By combining laser structuring with a thin PDMS coating, surfaces can be created that exhibit both low water and low ice adhesion (Figure 8) even after multiple de-icing cycles. In addition, the force required to remove adhering ice is even reduced after multiple mechanical de-icing cycles. Here, the dot structures show the most promising behavior. Even after multiple mechanical de-icing, the shear stress to overcome ice adhesion remains at similarly low levels to those found for PDMS coatings on unstructured aluminum.

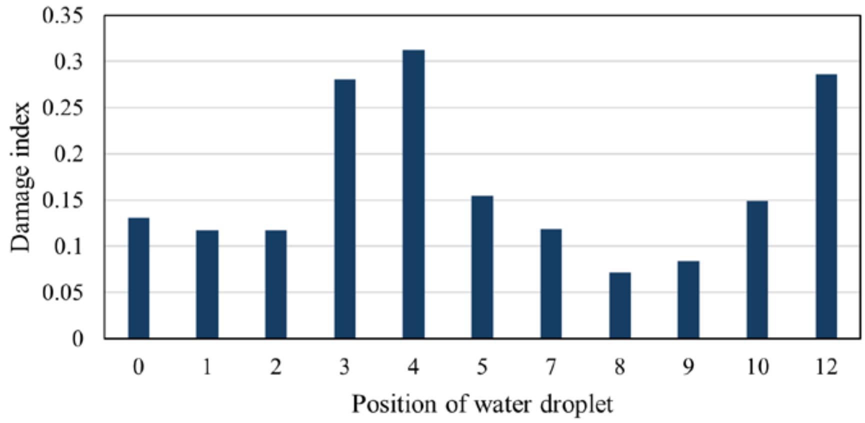

Figure 9. Calculated damage indices based on the correlation coefficient of the susceptance curves. A higher value corresponds to a higher deviation between the signal without water droplets and the signal of the condition with water droplets.

In addition to the anti-ice properties of fin surfaces, the detection of ice and water also plays a crucial role in the challenge of improving the energy efficiency of ASHPs through demand-based defrosting. Figure 9 shows calculated damage indices for measurements at an attached piezoelectric sensor as it was shown in Figure 3 when applying water droplets with 75µl at different positions. Taking the diagram into account, it can be concluded that even a very small amount of water can be detected in the surrounding area of a transducer using impedance analysis. The surrounding area is defined as positions 0 to 12. The highest damage indices, and thus the largest deviation in susceptance between a fin without water droplets and a fin with water droplets, are obtained when there are neither corrugations nor holes for tube passages between the transducer and the droplet position (Figure 3). However, no linear relationship can be observed between the distance of the droplet from the transducer and the magnitude of the damage index. Nevertheless, it can clearly be concluded that the detection is most sensitive to water droplets located in the immediate vicinity of the transducer.

4. Conclusion

Hierarchical superhydrophobic surfaces were successfully produced by DLIP and were shown to reduce water deposition on the fins under condensation- and frost-promoting climate conditions, leading to significantly smaller frost-layer thicknesses after 90 min compared to non-structured aluminum fins used as reference material. However, the structured surfaces cause the ice layer to adhere much more strongly, which will make mechanical removal very difficult. Dot structures produced by DLIP exhibit increased durability compared to pillar structures and can be applied to fin surfaces at higher processing speeds. Further investigations are necessary to identify the optimal surface modification and de-icing mechanism from the multitude of options and partly conflicting trends, aiming for solutions that provide beneficial effects over the widest possible range of operating conditions.

Coatings such as PDMS can be used to create surfaces that reduce ice adhesion, but these flexible coatings exhibit a deteriorating effect on the frosting behavior. Further tests on real heat pumps are required to determine which aspects of icing behavior have a decisive influence on the efficiency (COP) of an ASHP. The thermal conductivity of the resulting layers will also play a crucial role, but has not yet been considered in this work.

In addition, laboratory experiments demonstrated that water droplets can be successfully detected on fins by means of electromechanical impedance analysis.

Acknowledgements

This work was supported by the BMWE Federal Ministry for Economic Affairs and Energy Germany under Grant 03EN4066. The authors report there are no competing interests to declare. The authors gratefully acknowledge the project partners of the joint research project PIEZOdevICE Thomas Hackensellner and Andreas König-Haagen (Glen Dimplex Deutschland GmbH), Alfred Erhard and Martin Glatzer (Güntner GmbH & Co. KG), André Lienert (WiE GmbH), as well as Joachim Seifert and Lars Schinke (TU Dresden) for their valuable insights into industrial practice and the many helpful discussions related to the subject of this work.

References

[1] Deutsche Energie-Agentur (Hrsg.) (dena, 2023): DENA-GEBÄUDEREPORT 2024. Zahlen, Daten, Fakten zum Klimaschutz im Gebäudebestand.

[2] Kropas, T., Streckiené, G., Bielskus, J. Experimental Investigation of Frost Formation Influence on an Air Source Heat Pump Evaporator. *Energies* 2021, 14:5737

[3] Huang, L., Liu, Z., Liu, Y., Gou, Y., Wang, J. Experimental stuy on frost release on fin-and-tube heat exchangers by use of a novel anti-frosting paint. *Thermal and Fluid Science* 2009, 33

[4] Wang, W., Thang, S., Li, Z., Sun, Y. Deng, S., Wu, X. Determination of the Optimal Defrosting Initiating Time Point for an ASHP Unit Based on the Minimum Loss Coefficient in the Nominal Output Heating Energy. *Energy* 2020, 191:116505

[5] Klingebiel, J., Höges, C., Göbel, S., Bannmüller, P., Boelsen, T., Venzik, V., Vering, C. Müller, D. Optimal defrost initiation for air-source heat pumps: Evaluating the improvement potential of common defrosting controllers. *Energy* 2025, 324, 135871

[6] Pommier-Budinger, V., Budinger, M., Rouset, P., Dezitter, F., Huet, F., Wetterwald, M., Bonaccurso, E. Electromechanical Resonant Ice Protection Systems: Initiation of Fractrues with Piezoelectric Actuators. *AIAA Journal* 2018 56:11

[7] Shi, Z., Zhang J., Ultrasonic Guided Waves De-Icing System Feasibility Study. *13th Symposium on Piezoelectricity, Acousic Waves and Device Applications (SPAWDA)* 2019, 1-4

[8] Ramanathan, S., Varadan, VV, Varadan, VK, Deicing of helicopter blades using piezoelectric actuators. *Proc. SPIE 3990, Smart Structures and Materials 2000: Smart Electronics and MEMS* 2000

[9] Palacios, J., Smith, E., Rose, J., Instantaneous De-Icing of Freezer Ice via Ultrasonic Actuation. *AIAA Journal* 2011 49:6

[10] Shi, Z., Zhao, Y., Ma, C., Zhang J., Parametric Study of Ultrasonic De-Icing Method on a Plate with Coating. *Coatings* 2020, 10:7

[11] Liu, S., Bai, X., Zhang, L., Lin, Y., Shiming, D., Wang, W., Wei, M. Developing condensing-frosting performance maps for a variable speed air source heat pump (ASHP) for frosting suppression. *Applied Thermal Engineering* 2022, 118397

[12] Li, C., Apelt, S., Feuer, A., Idrisov, R., Bergmann, U. Bio-inspired surface modifications of aluminium heat exchanger fins using laser structuring and PDMS coating for improved and scalable hydrophobic and ice-adhesion performance. *The Journal of Adhesion* 2025, 1-16

[13] Li, R., Gu, Z., Zhang, Y., Li, Z., Lu, W., Luo, X., Wang, Z., Performance of air source heat pump units with different wettability evaporators. *Applied Thermal Engineering* 2024 257:124458

[14] Pan, R., Zhang, H., Zhong, M., Triple-Scale Superhydrophobic Surface with Excellent Anti-Icing and Icephobic Performance via Ultrafast Laser Hybrid Fabrication. *ACS Applied Materials & Interfaces* 2021, 13:1, 1743-1753

[15] Wang, F., Liang, C., Zhang, X., Zhang, Y., Effects of surface wettability and defrosting conditions on defrosting performance of fin-tube heat exchanger. *Experimental in Thermal and Fluid Science* 2018 93, 334-343

[16] Kim, K., Lee, KS, Frosting and defrosting characteristics of a fin according to surface contact angle. *International Journal of Heat and Mass Transfer* 2011, 54, 2758-2764

[17] Lasagni, AF, Gachot, C., Trinh, KE, Hans, M.,Rosenkranz, A., Roch, T., Eckardt, S., Kunze, T., Bieda, M., Günther, D., Lang, V., Mücklich, F. Direct laser interference patterning, 20 years of development:

from the basics to industrial applications. Proceedings Laser-based Micro- and Nanoprocessing XI; 2017 1009211

[18] Schnell, G., Piehl, J., Hartig, T., Dubhorn, N., Aliyeva, A., Springer, A., Strunskus, T., Faupel, F., Schröder, S., Seitz, H., PFAS-free superhydrophobic surfaces using femtosecond laser processing and hot-filament chemical vapor deposition. *Surfaces and Interfaces* 2025, 73, 107605

[19] Irajizad, P., Nazifi, S., Ghasemi, H. Icephobic surfaces: Definition and figures of merit. Advances in Colloid and Interface Science 2019, 269: 203-218

[20] Apelt, S., Bergmann, U. Insights into the Interface During Ice Adhesion Measurements. *Nano Express* 2023 5:1

[21] Mueller, I. *Inspection of piezoelectric transducers used for structural health monitoring systems*, PhD thesis, in Schriftenreihe der Arbeitsgruppe für Technische Mechanik, Universität Siegen, 2017

[22] Zhu, JH, Sun, YY, Wang, W., Deng, SM, Ge, YJ, Li, LT, Developing a new frosting map to guide defrosting control for air-source heat pump units. *Applied Thermal Energy* 2015, 90:782-791

[23] Butt, HJ, Liu, J., Koynov, K., Straub, B., Hinduja, C., Roismann, I., Berger, R., Li, X., Vollmer, D., Steffen, W., Kappl, M. Contact angle hysteresis. *Current opinion in Colloid & Interface Science* 2022, 59:101574